

Laser assisted Compton scattering of X-ray photons

D. Seipt^{1,2,*} and B. Kämpfer^{2,3}

¹*Helmholtz-Institut Jena, Fröbelstieg 3, 07743 Jena, Germany*

²*Helmholtz-Zentrum Dresden-Rossendorf, P.O. Box 510119, 01314 Dresden, Germany*

³*TU Dresden, Institut für Theoretische Physik, 01062 Dresden, Germany*

The Compton scattering of X-ray photons, assisted by a short intense optical laser pulse is discussed. The differential scattering cross section reveals the interesting feature that the main Klein-Nishina line is accompanied by a series of side-lines forming a broad plateau where up to $\mathcal{O}(10^3)$ laser photons participate simultaneously in a single scattering event. Due to the non-linear mixing of X-ray and laser photons a frequency dependent rotation of the polarization of the final state photons relative to the scattering plane emerges. A consistent description of the scattering process with short laser pulses requires to work with X-ray pulses. An experimental investigation can be accomplished, e.g., at LCLS or the European XFEL in the near future.

PACS numbers: 12.20.Ds, 32.80.Wr, 41.60.Cr, 13.60.Fz, 13.88.+e

Keywords: intense laser pulses, XFEL, laser assisted processes, Compton scattering, X-ray polarization

Introduction — Compton scattering [1], i.e. the scattering of X or γ rays off free electrons is one of the fundamental interaction processes of photons with charged particles. A particular feature is the dependence of the frequency ω'_{KN} of the scattered photon on the angle ϑ , $\omega'_{\text{KN}} = \omega_X / (1 + \frac{\omega_X}{m} [1 - \cos \vartheta])$, in the initial rest frame of the scattering particle with mass m . For linearly polarized X-rays the scattered photon polarization direction is the same as for electric dipole radiation. These properties become modified in laser assisted Compton scattering $X + L + e \rightarrow e' + X'$, where we suppose alignment of the X-ray beam (X , energy $\omega_X \sim \mathcal{O}(\text{keV})$) and an intense optical laser pulse (L , frequency $\omega_L \sim \mathcal{O}(\text{eV})$). The frequency ω' of the scattered photon X' in the initial rest frame of the electron e reads (with $\hbar = c = 1$)

$$\omega'(\ell, \vartheta) = \frac{\omega_X + \ell \omega_L}{1 + \frac{\omega_X + \ell \omega_L}{m} (1 - \cos \vartheta)}, \quad (1)$$

i.e. a non-linear frequency mixing occurs with the net number ℓ of laser photons involved. The value of ℓ may be positive or negative, where the latter case corresponds to a net emission of photons into the laser mode during the interaction. Obviously, $\ell = 0$ recovers the laser-free scattering of an X-ray photon with known Klein-Nishina (KN) kinematics. A large frequency ratio $\varkappa = \omega_X / \omega_L$ leads to a strong dynamical enhancement of non-linear multi-laser photon effects such that many side-lines form a broad plateau reaching to $|\ell| \gg 1$. Although the possibility of a strong enhancement was recognized in [2], the cross section for large values of ℓ and the corresponding cut-off values have never been calculated to the best of our knowledge. This gap will be filled in this letter, where we also take into account the finite lengths of both the X-ray and laser pulses.

The basic scattering process can be understood qualitatively in a classical picture, where the “slow” electron motion due to the laser is described classically. For high-intensity laser fields of the order of 10^{18} W/cm^2 the mo-

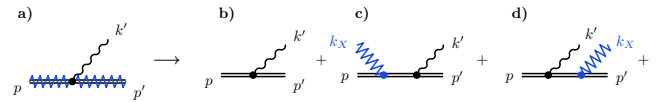


FIG. 1. (Color online) Expansion of the Feynman diagram (a) for photon emission off a dressed electron (double zig-zag line: electron in the combined laser and X-ray field, plain double line: electron in the laser background, wavy line: photon, and zig-zag line: X-ray) for a weak X-ray field in powers of a_X , yielding spontaneous emission (b), laser assisted Compton scattering (c) and induced emission (d).

tion of electrons becomes relativistic and non-linear, resembling a figure-8 motion with a velocity component in the laser beam direction [3, 4], superimposed to the usual transverse motion. In this picture, laser assisted Compton scattering corresponds to the scattering of X-rays off accelerated charges, and the broadening of the KN line occurs due to a time dependent Doppler shift induced by the figure-8 motion.

Observing the plateau of side-lines within a certain interval determined by cut-off values with special angular dependencies is a clear experimental signal for laser assisted Compton scattering of X-rays, i.e. a new possibility to observe $\mathcal{O}(10^3)$ multi-photon effects in strong-field QED. In addition, as we shall show below, the polarization properties of X' represent a new feature. The non-linear frequency mixing leads to a frequency dependent rotation of the polarization of the final state photons. This rotation does not affect the main KN line ($\ell = 0$) and is useful to identify the side-bands in an experiment. In the following, we describe the photon beams as a classical plane wave background field with four-vector potential $A^\mu = A_X^\mu(\varkappa\phi) + A_L^\mu(\phi)$, defining $\phi = k_L \cdot x \equiv k_L^\mu x_\mu$ with $k_L^\mu = (\omega_L, \mathbf{k}_L)$ and $k_X^\mu = \varkappa k_L^\mu$. We consider orthogonal linear polarizations, $A_X \cdot A_L = 0$. The vector potentials are parametrized as $A_j^\mu(\phi) = \frac{ma_j}{e} \epsilon_j^\mu g_j(\phi) \cos \phi$, $j \in \{X, L\}$, with the modulus of the electron charge e ,

normalized polarization vectors ϵ_j^μ and invariant laser strength parameters a_j . The envelope functions g_j account for the finite pulse lengths T_j of both the X-ray and the laser pulses and are assumed to be synchronized temporally. (This is new as compared to previous studies [2, 5–8]. The previous works were only for monochromatic waves and/or were restricted to non-relativistic intensities and relations for the cross section were calculated only for small values of ℓ [5–7], or were restricted to the angular distributions [8].)

For the given background field A^μ we may work in the Furry picture employing Volkov states $\Psi_p(x, A)$ [4, 9], as non-perturbative solutions of the Dirac equation. The S matrix for the emission of the photon X' with momentum k' is given by $S = -ie \int d^4x \bar{\Psi}_{p'}(x, A) \not{\epsilon}' e^{ik' \cdot x} \Psi_p(x, A)$, as depicted in Fig. 1(a). The non-perturbative expression, in both a_X and a_L , is correct for arbitrary X-ray and laser intensities. Even for present XFEL technology $a_X \ll 1$, and we may expand the S matrix into a power series in a_X to get $S \simeq S_0 + a_X(S_{+1} + S_{-1}) + \mathcal{O}(a_X^2)$. This corresponds to treating the field A_X as a perturbation [10]. (A similar technique has also been used in [11].) The lowest order term $S_0 \propto a_X^0$ (see Fig. 1(b)) corresponds to non-linear optical-laser Compton scattering without any participation of X-ray photon [12]. This scattering of laser photons off free electrons is named commonly non-linear Thomson or Compton scattering, see e.g. [13–19]. In the classical picture, this is the radiation due to the accelerated figure-8 motion of the electron in the laser. In the present context it may be dubbed spontaneous emission. Using moderately strong laser pulses with $a_L \sim 1$, the non-linear interaction with $\ell > 1$ photons has been verified experimentally [20, 21] via the observation of harmonic radiation. In these experiments, only a rather small number of $\mathcal{O}(2 \dots 5)$ laser photons was participating in a single scattering event.

The leading order process involving X-ray photons is proportional to a_X^1 and consists of two terms which correspond to the absorption (S_{+1} , Fig. 1(c)) or the emission (S_{-1} , Fig. 1(d)) of a single X-ray photon from or to the initial beam. The laser assisted Compton scattering is described by S_{+1} with energy-momentum conservation $k_X + \ell k_L + p = p' + k'$. In a pulsed laser field, the photon "number" ℓ can acquire nearly arbitrary real values [22]. The frequency ω' as a function of the scattering angle ϑ and the number of exchanged laser photons ℓ , Eq. (1), is derived from the above energy momentum conservation. The lower boundary of the variable ℓ is determined by the condition $\omega' \geq 0$, yielding $\ell \geq -\varkappa$. Due to the large frequency ratio the two partial processes (b) and (c) are separated kinematically: While photons from spontaneous emission S_0 have typical energies of $\omega' = \mathcal{O}(\text{eV})$ (Eq. (1) with $\omega_X = 0$), the photons from laser assisted Compton scattering S_{+1} are $\omega' = \mathcal{O}(\text{keV})$. The induced process S_{-1} , related to double Compton scattering [23], is strongly suppressed here in the keV frequency range

due to the large value of \varkappa .

Matrix element and cross section — Performing the space-time integrations, S_{+1} can be written as $S_{+1} = -4ie\pi^3 \int d\ell \delta^{(4)}(p + \ell k_L + k_X - p' - k') M(\ell)$ with

$$M(\ell) = \bar{u}_{p'} \left[V_1^X C_0(\ell) - \alpha_X \sum_{n=0}^2 V_n^L C_n(\ell) \right] u_p \quad (2)$$

and the free Dirac spinors obeying $(\not{p} - m)u_p = 0$ and $\bar{u}_p u_p = 2m$. The coefficients read $\alpha_j = ma_j[(\epsilon_j \cdot p')/(k_j \cdot p') - (\epsilon_j \cdot p)/(k_j \cdot p)]$, $V_0^L = \not{\epsilon}'$, $V_1^j = ma_j \frac{\not{\epsilon}_j \not{k}_j \not{\epsilon}'}{2k_j \cdot p'} + ma_j \frac{\not{\epsilon}' \not{k}_j \not{\epsilon}_j}{2k_j \cdot p}$ and $V_2^L = \frac{m^2 a_L^2 \epsilon' \cdot k_L}{2p \cdot k_L p' \cdot k_L} \not{k}_L$, where we employ Feynman's slash notation. Using the slowly varying envelope approximation for the X-ray pulse envelope g_X [18], the functions C_n in (2) are given by $C_n = \int_{-\infty}^{\infty} d\phi [g_L(\phi) \cos \phi]^n g_X(\varkappa\phi) e^{i \int^{\phi} d\phi' \psi(\phi')}$ with the dynamic phase

$$\psi(\phi) = \ell + \alpha_L g_L(\phi) \cos \phi + \beta_L [g_L(\phi) \cos \phi]^2 \quad (3)$$

and $\beta_L = m^2 a_L^2 k' \cdot k_L / [2(p \cdot k_L)(p' \cdot k_L)]$. We emphasize the necessity for including a finite X-ray pulse length T_X . Without g_X , the integral C_0 diverges for $\ell \rightarrow 0$, i.e. when no laser photons are exchanged, even after a regularization similar to [16]. This is no issue for non-linear Compton scattering since there $\ell = 0$ implies $\omega' = 0$ [18]. Here, however, the divergence for $\ell = 0$ is for the KN line. This behavior can be related to the scattering of X-ray photons during the time interval outside the laser pulse. Consequently, the time integrated probability for that partial process would diverge for $T_X \rightarrow \infty$. To get consistent results, we have to include a finite time interval also for the X-ray pulse, i.e. to work with wave packets. Accordingly, the cross section

$$\frac{d\sigma}{d\Omega d\omega'} = \frac{r_e^2}{8\pi \int_{-\infty}^{\infty} d\phi g_X(\phi)^2} \frac{\omega' |M(\ell)|^2}{(k_L \cdot p)(k_L \cdot p')}, \quad (4)$$

depending on spin and polarization variables, is normalized to the incident X-ray flux ($r_e \simeq 2.8 \text{ fm}$ is the classical electron radius). In the limit $a_L \rightarrow 0$, i.e. a vanishing laser field, we recover from (2) the KN matrix element and from Eq. (4) the KN cross section, however, both ones with the initial photon X described as a wave packet.

Energy spectra — The following numerical results are for an experiment which could be realized when combining an XFEL (e.g. LCLS or European XFEL) with an optical laser. That means, despite of the coherence properties, the XFELs are considered as sources of short, almost monochromatic X-ray photon pulses. For the sake of definiteness we specify $\omega_X = 5 \text{ keV}$ for the X-rays as well as an 800 nm Ti:Sapphire laser, i.e. $\omega_L = 1.55 \text{ eV}$. The planned Helmholtz international beamline for extreme fields (HIBEF) [24] at the European XFEL [25] will provide such a set-up. We envisage laser intensities $I \sim 10^{18} \text{ W/cm}^2$, where $a_L = 0.68 \sqrt{I [10^{18} \text{ W/cm}^2]}$.

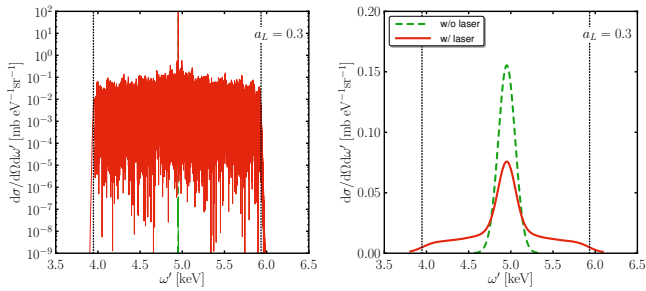


FIG. 2. (Color online) Differential cross section (left panel in a log scale) as a function of ω' for the fixed observation direction $\vartheta = 90^\circ$ and $\varphi = 45^\circ$ for $a_L = 0.3$. The vertical dotted lines depict the cut-off values (5). The right panel shows, in a linear scale, the spectrum with 100 eV (rms Gaussian shape) resolution (red solid curve; for a comparison, the plain KN line without the laser is depicted as green dashed curve).

The optical laser pulse length is set to $T_L = 20$ fs and the X-ray pulse length is taken as $T_X = 50$ fs (both FWHM values [26]), in agreement with routinely achieved optical laser pulses and XFEL design [25].

The unpolarized differential cross section is exhibited in Fig. 2 as a function of the frequency ω' for a fixed observation direction $\vartheta = 90^\circ$ and $\varphi = 45^\circ$. The scattering angle ϑ is measured w.r.t. the beam axis \mathbf{k}_L ; the azimuthal angle φ w.r.t. $\boldsymbol{\epsilon}_L$. In the left panel of Fig. 2, for $a_L = 0.3$ many side-lines form a roughened plateau, where the main KN line sticks out being very narrow as compared to the width of the plateau. The plateau spans the range 4...6 keV, corresponding to the order of $\ell \sim 1 \text{ keV}/\omega_L \sim 650$ exchanged laser photons, despite of $a_L < 1$. The right panel depicts the spectrum, averaged with a detector resolution of 100 eV, on a linear scale. While the KN line becomes broader, the plateau is clearly visible and the roughness is averaged out.

Multi-photon effects — To find the relevant multi-photon parameter for the process in Fig. 1(c) we determine the cut-off values ℓ_\pm , beyond which the amplitude drops exponentially fast, via the stationary phase method by requiring that there are no stationary points ϕ_\star on the real axis, i.e. $\psi(\phi_\star) = 0$ (see Eq. (3)) has no real solutions. Abbreviating $f = g_L(\phi) \cos \phi$ we find $f(\phi_\star) = -\alpha_L/2\beta_L \pm (\alpha_L^2/4\beta_L^2 - \ell/\beta_L)^{1/2}$, which has no real solutions for ϕ_\star if (i) the term under the root becomes negative or (ii) there are no real solutions when calculating the inverse function f^{-1} . The cut-off values are determined at maximum intensity at the center of the pulse, thus, we may set $g_L \rightarrow 1$ here and condition (ii) turns into $|f| \leq 1$. We find

$$\ell_- = \frac{\varkappa\xi_-}{1 - \xi_-}, \quad \ell_+ = \begin{cases} \frac{\varkappa\xi_+}{1 - \xi_+}, & \text{for } \vartheta \leq \vartheta_\star, \\ \frac{\varkappa\xi_0}{1 - \xi_0}, & \text{for } \vartheta > \vartheta_\star \end{cases} \quad (5)$$

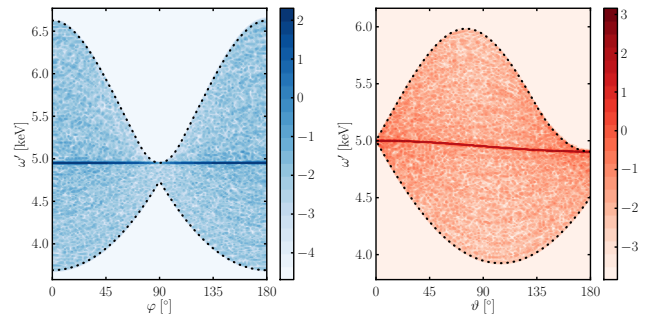


FIG. 3. (Color online) Frequency vs. angle correlations of the cross section as a function of the azimuthal angle for fixed $\vartheta = 90^\circ$ (left panel) and as a function of ϑ for fixed $\varphi = 45^\circ$ (right panel) for $a_L = 0.3$. The cutoff-values (5) are depicted by the dotted curves. The color scale represents $\log_{10}(d\sigma/d\Omega d\omega' [\text{mb eV}^{-1}\text{sr}^{-1}])$.

with $\xi_0 = \frac{\sin^2 \vartheta \cos^2 \varphi}{2 - 2 \cos \vartheta}$, $\xi_\pm = \frac{a_L^2}{2} (\cos \vartheta - 1) \pm a_L \sin \vartheta \cos \varphi$ and $\cos \vartheta_\star = (a_L^2 - \cos^2 \varphi)/(a_L^2 + \cos^2 \varphi)$. For $a_L < 1$, the cut-off values are of the order $a_L \varkappa$ for most observation angles. Thus, for moderately strong laser fields and a large frequency ratio the relevant multi-photon parameter is $\varkappa a_L$. This is in severe contrast to the spontaneous process S_0 depicted in Fig. 1(b), where the multi-photon parameter is a_L [27].

Angular spectrum — The plateau has a pronounced dependence on the azimuthal angle φ , see left panel of Fig. 3. A strong reduction of the plateau width is observed at $\varphi = 90^\circ$, i.e. perpendicularly to the laser polarization, where $\ell_+ = 0$. The broadest plateau is found close to the laser polarization direction which is perpendicular to the X-ray polarization where up to 1000 laser photons participate. The polar angle distribution (right panel) shows a forward-backward asymmetry. For large scattering angles $\vartheta > 90^\circ$ the emission with $\ell > 0$, i.e. $\omega' > \omega'_{\text{KN}}$ is suppressed. The cut-off values (5), depicted by dotted curves, coincide with the numerical results. The preferred observation direction is $\vartheta = 90^\circ$ and $\varphi = 45^\circ$, as discussed above in Fig. 2.

Total probability — Numerically we find that the energy integrated cross section equals the KN cross section [28], i.e. $\frac{d\sigma}{d\Omega} = \frac{d\sigma_{\text{KN}}}{d\Omega}$. A qualitative argument for this behavior is provided by a classical model, where the total emitted power \dot{E} is given by the Larmor formula yielding $\dot{E} = -\frac{e^4}{6\pi m^2} (A'_L \cdot A'_L + A'_X \cdot A'_X)$. The first term in brackets corresponds to the spontaneous emission process and the second term refers to the laser assisted Compton scattering of X-ray photons S_{+1} . The latter part is independent of the laser intensity. Such a redistribution in phase space with marginal impact on the total probability has been found also for other laser assisted processes [29].

Sideband fraction — To quantify the fraction of photons scattered into the side-bands, in particular for the observation direction used in Fig. 2, we define the side-band

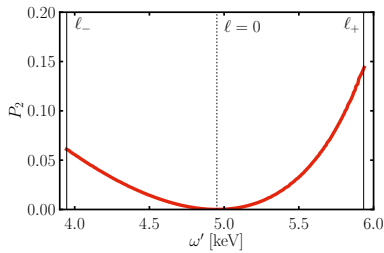


FIG. 4. (Color online) Rotation of the polarization of the scattered photon, quantified via the Stokes parameter P_2 as a function of ω' for the same observation direction as in Fig. 2.

cross section as that part of the spectrum which is at least by $\pm\omega_L/2$ away from ω'_{KN} . (A variation of the discrimination value in the range $0.25 \dots 0.75 \omega_L$ leads to a relative uncertainty of $\leq 5\%$.) For small values of $\varkappa a_L \ll 1$, the side-band fraction scales as a_L^2 . For larger values of a_L , the main line is weakened, see right panel in Fig. 2. (For monochromatic waves, where $g_{X,L} \rightarrow 1$, also a negative lowest-order a_L corrections to the main line has been found [6, 7]). The side-band cross section increases with a_L up to $a_L \sim 0.01$, where it saturates at 30 mb sr^{-1} . This value should be compared to the corresponding KN cross section of 39 mb sr^{-1} , proving that a large fraction of the photons is emitted into the side-bands.

Polarization — Due to the non-linear mixing of optical laser photons with the incident X-ray photon the polarization of the photon X' is rotated as compared to Compton scattering without the laser. The rotation angle is frequency dependent. This rotation can be quantified experimentally by measuring the Stokes parameter P_2 which we calculate as $P_2 = (w_{45^\circ} - w_{135^\circ}) / (w_{45^\circ} + w_{135^\circ})$, where w_χ denotes the triple differential cross section of photons with their polarization vector having an angle of χ w.r.t. the scattering plane. For instance, for the observation angles of Fig. 2 the photon X' is polarized perpendicular to the scattering plane without the laser which means $P_2 = 0$. This result is changed in laser assisted Compton scattering. In Fig. 4 the Stokes parameter P_2 is exhibited as a function of ω' for $a_L = 0.3$. The value of P_2 is zero at the KN line and increases with increasing distance from it, i.e., in the region where more laser photons are involved. The maximum value of P_2 corresponds to a rotation angle of 5° towards \mathbf{k}_L . In the classical picture, the figure-8 orbit in the laser field has a component in the directions of \mathbf{k}_L which is transferred to the polarization of the photon X' . The energy dependent polarization rotation can be used to identify unambiguously the final state photons emerging from the multi-photon process.

Discussion and Summary — A clear and easily observable signature of laser assisted Compton scattering of X-ray photons is provided by the side-lines accompanying the main Klein-Nishina line forming a broad plateau.

Due to the difference of scales of the photon energies of X-ray and optical laser, non-linear effects are strongly enhanced as compared to the spontaneous emission of radiation in a pure laser field. The relevant multi-photon parameter is $\varkappa a_L$, which can be large even for laser fields with intensities of the order of 10^{18} W/cm^2 . The optimal conditions to observe the side-band plateau with an X-ray camera are achieved for $a_L \lesssim 1$. Such intensities are achieved routinely with a 200 TW laser in relatively large spot sizes of $\mathcal{O}(100 \mu\text{m})$ and pulse lengths of $T_L = 20 \text{ fs}$. We do not expect that spatially inhomogeneous laser spots influence the cut-off values since they are sensitive to the maximum laser intensity in the spatio-temporal profile of the pulse. However, the shape of the plateau will certainly change. The optical photons emerging from spontaneous emission process, i.e. the non-linear Compton process exhibited in Fig. 1(b), can be efficiently filtered out by a thin foil which is otherwise transparent for X-rays.

A very useful signal for the non-linear frequency mixing is the frequency dependent rotation of the polarization of the final state photons. The polarization can be measured by using X-ray polarizers. A polarization purity of the order of 10^{-10} has been achieved recently [30]. The technique of a polarization veto can be used to shield the plain KN photons (arising for unsynchronized X and L pulses) or shield the $\ell = 0$ KN-like photons. For optimal conditions, the X-ray pulse length T_X and the laser pulse length T_L should be of the same order of magnitude. The synchronization of optical and X-ray pulses to the level of femtoseconds has been achieved experimentally [31], approaching the sub-femtosecond level [32]. Numerically, the spectra are insensitive to a temporal offset between the two pulses of the order of a few femtoseconds.

A slight misalignment of the X-ray and laser beams due to axis off-sets or focusing effects does not lead to qualitatively new effects: The Oleinik resonances [5] for non-parallel beams (see e.g. [33, 34]) are suppressed by the large frequency ratio \varkappa and for a small angular misalignment $\Theta \ll 1$ between the X-ray and laser beams. A slight misalignment of the polarizations, $\epsilon_X \cdot \epsilon_L \neq 0$, causes laser intensity dependent modifications of the total cross section of the order $\mathcal{O}(\epsilon_X \cdot \epsilon_L) \ll 1$.

Such experiments can be performed at LCLS or at the European XFEL combining the X-ray facility with an optical laser system, e.g., as planned in HIBEF [24]. One could employ low-energy electrons emitted from an electron gun as in the experiment [20].

In conclusion, studying the laser assisted Compton scattering of X-rays will significantly advance our understanding of strong-field QED scattering processes in the $\mathcal{O}(10^3)$ multi-photon regime.

Acknowledgements — The authors are grateful to T. E. Cowan and R. Sauerbrey for the inspiring collaboration on future experiments at HIBEF. DS acknowledges stimulating discussions with S. Fritzsche, A. Surzhykov

and V. G. Serbo.

* d.seipt@gsi.de

- [1] A. H. Compton, Phys. Rev. **21**, 483 (1923).
- [2] F. Ehlotzky, J. Phys. B **20**, 2619 (1987).
- [3] E. S. Sarachik and G. T. Schappert, Phys. Rev. D **1**, 2738 (1970).
- [4] A. Di Piazza, C. Müller, K. Z. Hatsagortsyan, and C. H. Keitel, Rev. Mod. Phys. **84**, 1177 (2012).
- [5] V. P. Oleinik, Sov. Phys. JETP **26**, 1132 (1968).
- [6] R. Guccione-Gush and H. P. Gush, Phys. Rev. D **12**, 404 (1975).
- [7] A. I. Akhiezer and N. P. Merenkov, Sov. Phys. JETP **61**, 41 (1985).
- [8] A. K. Puntajer and C. Leubner, Phys. Rev. A **40**, 279 (1989).
- [9] D. M. Volkov, Z. Phys. **94**, 250 (1935).
- [10] J. Herrmann and V. C. Zhukovskii, Ann. Phys. (Leipzig) **482**, 349 (1972).
- [11] H. Hu and C. Müller, Phys. Rev. Lett. **107**, 090402 (2011).
- [12] There are corrections to that process of the order of a_X^2 when arranging the expansion of Fig. 1(a) according to the energy-momentum balance $\ell k_L + p = p' + k'$ [10].
- [13] L. S. Brown and T. W. B. Kibble, Phys. Rev. **133**, A705 (1964).
- [14] N. B. Narozhnyi, A. I. Nikishov, and V. I. Ritus, Sov. Phys. JETP **20**, 622 (1965); N. B. Narozhnyi and M. S. Fofanov, JETP **83**, 14 (1996).
- [15] C. Harvey, T. Heinzl, and A. Ilderton, Phys. Rev. A **79**, 063407 (2009).
- [16] M. Boca and V. Florescu, Phys. Rev. A **80**, 053403 (2009).
- [17] T. Heinzl, D. Seipt, and B. Kämpfer, Phys. Rev. A **81**, 022125 (2010).
- [18] D. Seipt and B. Kämpfer, Phys. Rev. A **83**, 022101 (2011).
- [19] F. Mackenroth and A. Di Piazza, Phys. Rev. A **83**, 032106 (2011).
- [20] T. J. Englert and E. A. Rinehart, Phys. Rev. A **28**, 1539 (1983).
- [21] C. Bula *et al.*, Phys. Rev. Lett. **76**, 3116 (1996); S.-Y. Chen, A. Maksimchuk, and D. Umstadter, Nature **396**, 653 (1998).
- [22] A. Ilderton, Phys. Rev. Lett. **106**, 020404 (2011).
- [23] E. Lötstedt and U. D. Jentschura, Phys. Rev. Lett. **103**, 110404 (2009); D. Seipt and B. Kämpfer, Phys. Rev. D **85**, 101701 (2012); F. Mackenroth and A. Di Piazza, Phys. Rev. Lett. **110**, 070402 (2013).
- [24] “The HIBEF project,” www.hzdr.de/hgfbeamline/.
- [25] “The European XFEL project,” <http://www.xfel.eu/>.
- [26] For convenience we use a \cos^2 profile for g_L and a Gaussian for g_X .
- [27] V. I. Ritus, J. Sov. Laser Res. **6**, 497 (1985).
- [28] W. B. Berestetzki, E. M. Lifschitz, and L. P. Pitajewski, *Relativistische Quantentheorie*, Lehrbuch der Theoretischen Physik, Vol. IV (Akademie Verlag, Berlin, 1980).
- [29] E. Lötstedt, U. D. Jentschura, and C. H. Keitel, Phys. Rev. Lett. **101**, 203001 (2008).
- [30] B. Marx *et al.*, Phys. Rev. Lett. **110**, 254801 (2013).
- [31] F. Tavella, N. Stojanovic, G. Geloni, and M. Gensch, Nature Photon. **5**, 162 (2011).
- [32] M. Schultze *et al.*, Science **328**, 1658 (2010).
- [33] A. Hartin, *Second Order QED Processes in an Intense Electromagnetic Field*, Ph.D. thesis, University of London (2006).
- [34] A. I. Voroshilo and S. P. Roshchupkin, Laser Phys. Lett. **2**, 184 (2005); A. I. Voroshilo, S. P. Roshchupkin, and V. N. Nedoroshta, Laser Phys. **21**, 1675 (2011).